DETECTION OF OPTICAL FREQUENCIES OF METAL-OXIDE-METAL JUNCTIONS

by

Sırma Başak Yanardağ

BS., in Phys., Boğaziçi University, 2005

Submitted to the Institute for Graduate Studies in
Science and Engineering in partial fulfillment of
the requirements for the degree of
Master of Science

Graduate Program in Physics
Boğaziçi University
2008

ACKNOWLEDGEMENTS

I would like to thank several people without whom I would not able to complete this thesis. My foremost thank goes to my thesis advisor Prof. Yani Skarlatos. Without him, this thesis would not have been possible. I thank him for his patience and encouragement that carried me on through difficult times, and for his insights and suggestions that helped to shape my research skills. His valuable feedback contributed greatly to this thesis. I am also grateful to Prof. Naci İnci, who advised me and helped me in various aspects of my research. I would also like to thank Assist. Prof. Şenol Mutlu for being in my thesis committee.

I thank my labmates Arzu, İbrahim, Aydın, Sabriye. They helped me to improve this thesis in many ways. My special thanks go to my friends Ahmet, Cem, Neslihan, Burcu, Cemile, Serhat, Kaan, Erkal, Kamber and Taylan. They were always kind and helpful, their support is very valuable for me.

Finally, I am forever indebted to my parents for their understanding, endless patience and encouragement when it was most required. I am also grateful to Pınar, Fırat and Umut for their presence and support.

ABSTRACT

DETECTION OF OPTICAL FREQUENCIES OF METAL-OXIDE-METAL JUNCTIONS

In this thesis, optoelectronic characteristics of metal-oxide-metal junctions are investigated. The junctions are made of aluminum. The detected current in the $Al - Al_2O_3 - Al$ films is due to a quantum mechanical phenomena; tunneling. Classically, if the energy of the particle is less than the height of the barrier, the particle can never pass through it. However, in quantum mechanics the electrons can penetrate into a classically forbidden region without any real tunnel even when its energy is smaller than the height of the barrier. The tunneling current depends on the thickness of the insulator, the work function of aluminum, and the applied voltage.

ÖZET

METAL-OKSİT-METAL KAVŞAKLARININ OPTİK FREKANSLARININ SAPTANMASI

Bu tezde, aluminyum kullanılarak yapılan metal-oksit-metal kavşakların optoelektronik karakteristikleri incelenmiştir. $Al - Al_2O_3 - Al$ filmlerinde saptanan akım, quantum mekaniğiyle açıklanan bir olgu olan tünel olayının sonucudur. Klasik olarak bir parçacığın enerjisi, bariyerin enerjisinden küçük olursa parçacık o bariyeri hiçbir zaman geçemez. Ancak quantum mekaniğinde, elektronun enerjisi bariyerin enerjisinden küçük olsa bile, elektron bir yalıtkan yasak bandının oluşturduğu engeli gerçek bir tünel açmadan geçer. Oksit tabakasının kalınlığı, aluminyum metalinin iş fonksiyonu ve uygulanan voltaj, tünel akımını etkileyen parametrelerdir.

TABLE OF CONTENTS

ACKNOWLEDGEMENTS . . . iii
ABSTRACT . . . iv
ÖZET . . . v
LIST OF FIGURES . . . vii
LIST OF SYMBOLS/ABBREVIATIONS . . . x
1. INTRODUCTION . . . 1
2. THEORY . . . 3
2.1. Tunneling . . . 3
2.1.1. Basic Tunneling Theory . . . 3
2.1.2. Inelastic Tunneling . . . 4
2.1.3. Conduction Mechanisms . . . 6
2.1.4. Tunneling Between Dissimilar Electrodes . . . 8
2.2. A Simple Model . . . 10
2.3. Free Electron Tunneling . . . 13
2.4. Evaluation of the Tunneling Probability . . . 17
2.5. Calculation of the Tunneling Current . . . 18
2.5.1. The Influence of Image Force . . . 20
3. EXPERIMENTAL WORK AND RESULTS . . . 23
3.1. Sample Preparation . . . 23
3.1.1. Evaporation . . . 24
3.1.2. Oxide Barrier . . . 25
3.1.2.1. Thermal Oxidation . . . 25
3.1.2.2. Glow Discharge Oxidation . . . 26
3.2. Measurement of I-V Characteristics . . . 28
3.3. Measurement of Optoelectronic Characteristics . . . 28
3.3.1. Lock-in Amplifiers . . . 30
4. CONCLUSION . . . 34
REFERENCES . . . 35

LIST OF FIGURES

Figure 2.1. The schematic drawing of tunneling experiment 3

Figure 2.2. Energy diagram for two identical metals separated by a potential barrier of height Φ and width s. (a) No voltage applied. (b) Voltage V applied electrons can tunnel from metal 1 to metal 2 4

Figure 2.3. Inelastic process provides an additional channel for current flow, so one sees a break in the I-V curve [10] 5

Figure 2.4. Energy diagram of a M-I-M junction, showing (a) elastic and (b) inelastic tunneling[13] 6

Figure 2.5. Schematic representation of the band structure of a metal-insulator-metal junction with voltage V is applied to it. The six mechanisms of conduction through junction are indicated [15] 7

Figure 2.6. Energy diagram of potential barrier between similar electrodes . . 9

Figure 2.7. Energy diagram of potential barrier between dissimilar electrodes [20] 9

Figure 2.8. Typical curve shapes for free electron (nonsuperconducting state) tunneling at T=0. (a) Current-Voltage (b) Resistance-Voltage (c) Conductance-Voltage. The dashed curves schematically indicate the effect of finite temperature [21]. 12

Figure 2.9. A potential step of height V_0 13

Figure 2.10. Free electron tunneling through one dimensional square-well potential 14

Figure 2.11. General tunneling problem. The wave functions, Ψ and $d\Psi/dx$ must be matched at x = 0 and x = s 18

Figure 2.12. Normalized energy diagram comparing a parabolic approximation with true barrier for zero voltage bias [28] 21

Figure 2.13. Normalized energy diagram comparing a parabolic approximation with true barrier for zero voltage bias of 1 eV [6] 22

Figure 3.1. Preparation of an Al-Al_2O_3-Al sandwich. (a) Glass slide with indium contacts. (b) An aluminum strip has been deposited across the contacts. (c) The aluminum strip has been oxidized to form an Al_2O_3 layer. (d) A film has been deposited across the film, forming an Al-Al_2O_3-Al sandwich. The external leads are connected to the indium contacts; two contacts are used for the current measurement and two for the voltage measurement [22]. 24

Figure 3.2. The glow discharge oxidation method 27

Figure 3.3. The set-up used for I-V measurement 29

Figure 3.4. I-V characteristics of a typical junction 29

Figure 3.5. The set-up used for the measurement of the optoelectronic characteristics 31

Figure 3.6. dI/dV vs V for a typical junction 31

Figure 3.7. $d^2I/dV^2 vsV$ for a typical junction 32

Figure 3.8. The assumed shape of the junction[12] 32

Figure 3.9. The edges of the junction is covered with Al films[12] 33

LIST OF SYMBOLS/ABBREVIATIONS

$\mathring{A}$	Angstrom
Ag	Silver
Al	Aluminum
Au	Gold
Cd	Cadmium
Cr	Chromium
$D(E, k_r)$	Tunneling probability
e	Charge of electron
E	Energy of the electron
E_a	Activation energy
E_f	Fermi energy
E_m	Maximum energy of the electrons
$f(E)$	Fermi-Dirac function
F_i	Intrinsic field
G	Conductance
Ge	Germanium
$\hbar$	Planck's constant
I	Tunneling current
j_1	Current incident on the barrier
j_3	Transmitted current
J	Tunnel current density
k	Boltzmann constant
L_1	Length of the square well
m	Mass of electron
Mg	Magnesium
Nb	Niobium
Ni	Nickel
$n(v_x)dv_x$	Number of electrons per unit volume with velocity between v_x and $v_x + \mathrm{d}v_x$

N_1	Number of electrons tunneling from electrode 1 to electrode 2
N_2	Number of electrons tunneling from electrode 2 to electrode 1
O	Oxygen
Pb	Lead
R	Differential Resistance
R_T	Tunneling resistance
s	Thickness of the insulating film
S	Sulfur
Si	Silicon
Sn	Tin
T	Temperature
Ta	Tantalum
V	Height of the barrier
w	Thickness of the barrier
Zn	Zinc
η	Fermi level
κ	Wave vector
ν	Vibrational frequency
φ_1	Barrier height at the interface of electrode 1 and the insulator
φ_2	Barrier height at the interface of electrode 2 and the insulator
φ	Work function
Φ	Height of the barrier
Ψ_1	Height of the electrode 1
Ψ_2	Height of the electrode 2
$\Psi(x)$	Wave function
BCS	Bardeen Cooper Schrieffer
$I-V$	Current-Voltage
$M-I-M$	Metal-insulator-metal
$M-O-M$	Metal-oxide-metal

WKB	Wentzel Kramers Brillouin

1. INTRODUCTION

The concept of the flow of electrons through sufficiently thin insulating film arises from the theory of quantum mechanics. When a classic particle on a barrier of height V, it has 100 per cent probability of transmission if its energy $E > V$, and will be reflected with 100 per cent probability if its energy $E < V$. Conversely, in quantum mechanics; if the barrier is thin enough, an electron has a finite probability of tunneling through the insulator -classically forbidden region- without any real tunnel even when $E < V$ [1].

The concept of tunneling is as old as quantum mechanics. After Schrödinger's equation, the first application was made by Oppenheimer; he described the autoionization of excited states of atomic hydrogen in a strong electric field in 1928 [2]. The following applications are, field emission from a free-electron metal by Fowler and Nordheim(1928), alpha decay by Gamow(1928), metal-vacuum-metal junctions by Frenkel(1930), metal-insulator-metal junctions by Sommerfield and Bethe(1933) [3].

Between 1930-1945 the predictions were made about tunneling through thin insulating films between metals and semiconductors in solids. However, observations of tunneling became possible with the development of material technology during 1940s and early fifties [2]. The tunneling of electrons gain importance after the discovery of transistors in 1947. The construction of semiconductors like Ge and Si made possible to manufacture of semiconductors of given characteristics in 1950.

Up to the late fifties only physicists were interested in tunneling phenomena. In 1957 invention of Esaki Diode brought the attention of engineers to this issue [3]. This led to a considerable amount of work, improved technology and helped to spread an interest in the concept of tunneling. Tunneling has been the basis of a family of solid state devices.

Discovery of tunneling into superconductors came in 1960 by Giaever and Nicol, Shapiro and Smith. According to Giaever's observations, if one or both of the metals are superconductors, the I-V characteristics give interesting information concerning the state of superconductor(s). By the experiment of Giaever, it became possible to measure the energy gap in superconductors. This gap appears when electrons form Cooper pairs, and the gap plays an essential role in the BCS theory of superconductivity [4].

The Josephson tunneling, which is a new type tunneling and one of the major theories, was predicted by B.D. Josephson [5]. He predicted the existence of a second current, the supercurrent, in addition to the current found by Giaever. He showed that the second current was due to the tunneling of electrons in pairs.

The objective of this study is to detect the optical frequencies of metal-oxide-metal junctions. The samples used in experiments are $Al - Al_2O_3 - Al$ type.

In Chapter 2, basic tunneling theory, free electron model, conduction mechanisms, tunneling probability, calculation of tunneling current and image force are explained.

In Chapter 3, the experimental set up, the devices used, the measurements and their result are explained.

And in Chapter 4, a brief summary of the study and conclusions is presented.

2. THEORY

2.1. Tunneling

The current can flow through the insulating region between two electrodes if,

(i) the electrons in the electrode have sufficient energy to pass over the potential barrier and flow in the conduction band;

(ii) the barrier is thin enough to permit current flow between the two electrodes [6].

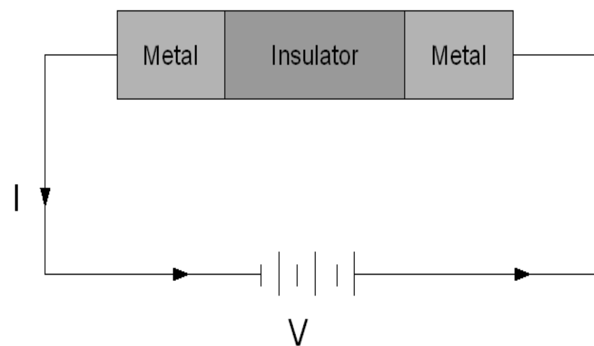

Figure 2.1. The schematic drawing of tunneling experiment

2.1.1. Basic Tunneling Theory

The tunneling theory in solids is one of the simplest examples of quantum mechanics. Classically, if the energy of the particle is less than the height of the barrier, particle can never pass through it. However, if the barrier is sufficiently thin ($< 30\mathring{A}$); and if a potential difference V is applied between the electrodes, the metal wave func-

tion can extend on the barrier, and thus, electron passes from one metal to the other.

Metals contain large number of free electrons. It is viewed simply as a box filled with electrons up to the energy E_f, called fermi energy. Since the electrons do not escape from the metal, some energy φ, is required to remove an electron. This energy is called the work function. When a potential V is applied across the vacuum gap, this separates the fermi energy in two metals by an energy eV. Electrons can find empty state on the other side with the same energy. Usually -but not always- the tunneling electron conserves its energy [7].

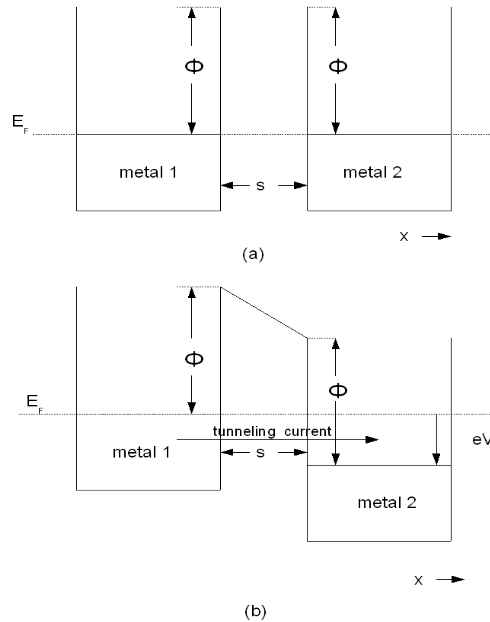

Figure 2.2. Energy diagram for two identical metals separated by a potential barrier of height Φ and width s. (a) No voltage applied. (b) Voltage V applied electrons can tunnel from metal 1 to metal 2

2.1.2. Inelastic Tunneling

In elastic tunneling processes, the tunneling electrons conserve their momentum in x-direction and also their energy [2]. However, sometimes tunneling electrons interact

with excitations of the oxide and the electrodes or with impurities present in the oxide, and afterwards the electrons lose energy [8]. As a result, the electrons tunnel to a lower state in the metal on the other side.

If the above mentioned mechanism has a characteristic energy $h\nu$, inelastic tunneling will occur for energies greater than $h\nu$. For energies lower than $h\nu$, there are no available empty states which the electrons can tunnel [8]. At energy $h\nu$, an additional channel for tunneling is opened up, and a decrease in the tunneling resistance can be observed [9].

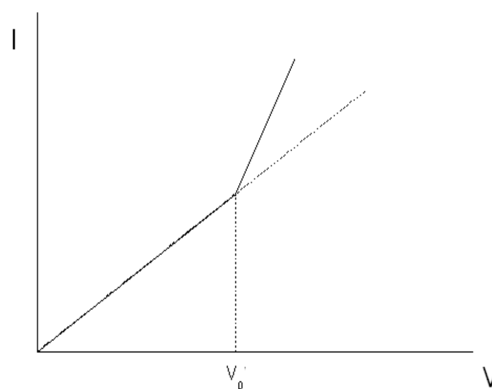

Figure 2.3. Inelastic process provides an additional channel for current flow, so one sees a break in the I-V curve [10]

In the case of a molecular excitation, the lost energy goes to the vibrational modes of the molecular species in the barrier. A break in the I-V curve (see Figure 2.3) can be seen at the threshold $V_0 = \frac{h\nu}{e}$, where ν is the vibrational frequency [11]. These vibrations are below the thermal vibrations, thus the observations are available only at liquid helium temperature [12].

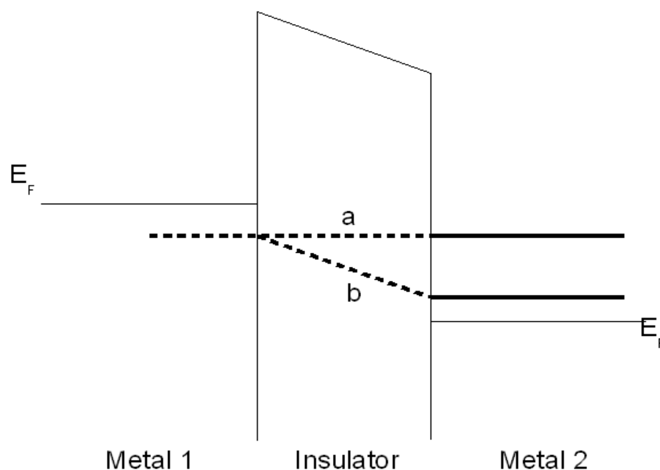

Figure 2.4. Energy diagram of a M-I-M junction, showing (a) elastic and (b) inelastic tunneling[13]

2.1.3. Conduction Mechanisms

Measurements on Al_2O_3 films showed that direct tunneling is the dominant conduction for the films less than $100\AA$ thick. In contrast, thermionic currents have been predominantly observed in films thicker than $100\AA$ [14].

Current flow through a thin insulating region between two metal contacts can be due to a number of different mechanisms. Some of these are indicated schematically in figure 2.5.

Direct tunneling of electrons from one metal to the other (a) depends on the thickness of the insulator. *Injection of carriers into the conduction (or valence) band of the insulator* (b) can take place by thermionic (Schottky) emission over a contact barrier or by *tunneling through that barrier (field emission)* (c). Thermionic emission occurs at high temperatures and low fields conversely, field emission takes place at high fields and

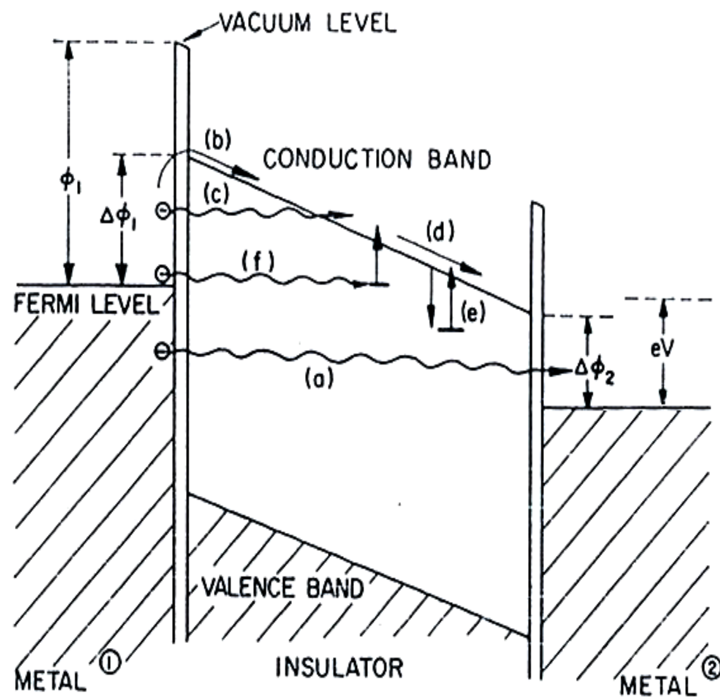

Figure 2.5. Schematic representation of the band structure of a metal-insulator-metal junction with voltage V is applied to it. The six mechanisms of conduction through junction are indicated [15]

low temperatures [16]. These two processes are analogous to the emission from a metal into vacuum. In both cases, Fermi-Dirac Statistics are valid, and one considers metal electrons as free particles which have to surmount the insulator. Thermionic emission occurs by the tunneling of the thermally excited electrons, however, field emission is possible only by quantum mechanical tunneling [17].

Carrier flow in the conduction band (d) depends on scattering mechanisms. The effect of carrier flow is small since very small distances are involved. *Trapping at impurities and imperfections* (e) is important in amorphous layers, because they contain large densities of traps. Trapped charge changes the space-distribution in the insulator and change the tunneling probability by many orders of magnitude. Any trapping effects relies on the ratio of free to trapped carriers, and it is temperature dependent. *The electrons can tunnel from the metals directly into the traps* (f). This would allow a build up of space charge which is temperature-independent[15].

2.1.4. Tunneling Between Dissimilar Electrodes

If the electrodes are similar, the potential barrier is symmetric [18].Yet, if the electrodes are dissimilar, there is an intrinsic field F_i. It exists because of the contact potential difference between two electrodes of different work functions [19].

$$F_i = \frac{\left(\Psi_2 - \Psi_1\right)}{es} \tag{2.1}$$

where s is the thickness of the insulator, and e is the charge of the electron. This field F_i produces an asymmetric potential barrier between two electrodes.

The energy diagram of dissimilar electrode is not constant but trapezoidal, as shown in figure 2.6. If we assume φ_1 is the barrier height at the interface of the electrode 1 and the insulating film, φ_2 at the interface of electrode 2 and the insulating

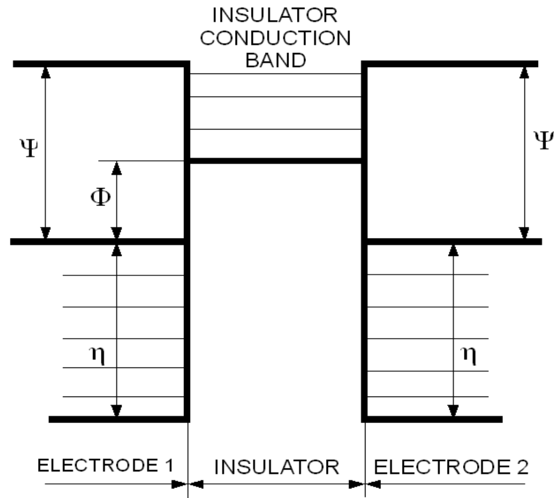

Figure 2.6. Energy diagram of potential barrier between similar electrodes

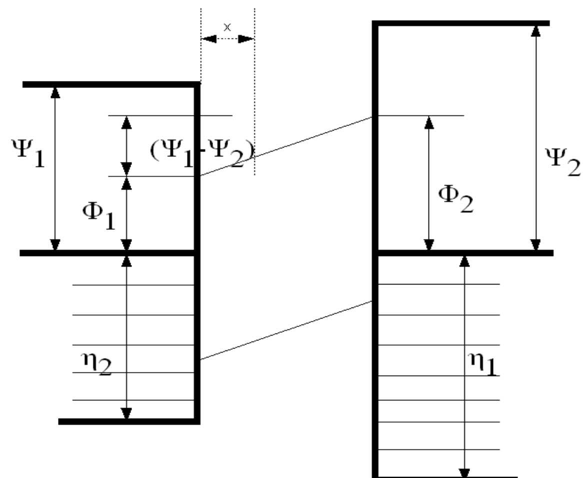

Figure 2.7. Energy diagram of potential barrier between dissimilar electrodes [20]

film, the barrier heights are related as [20],

$$\begin{aligned}\varphi_2 &= \varphi_1 + eF_i s \\ &= \varphi_1 + \Psi_2 - \Psi_1 \\ &= \varphi_1 + \Delta\Psi\end{aligned} \tag{2.2}$$

where,

$$\Delta\Psi = \Psi_2 - \Psi_1. \tag{2.3}$$

The height of the barrier $\varphi(x)$ is,

$$\varphi(x) = \varphi_1 + x\Delta\Psi/s. \tag{2.4}$$

2.2. A Simple Model

Let's consider two metals with a barrier of height Φ, and thickness s, at zero temperature. The metal can be assumed as free electrons of mass moving in one dimension. It is viewed as a finite square-well, filled up to the fermi level E_F. All states above E_F are empty. If $V = 0$, there will be no current flow, since the electrons on one side cannot find any available states to occupy. When a potential V is applied across the barrier, this causes the Fermi levels in the two metals to be separated by an energy eV. Hence, the electrons in one side can find empty states in the other side to occupy.

The transmission coefficient of a tunneling electron depends exponentially onto the thickness of the barrier and onto the square root of the height of the barrier. If small biases are applied to the metals, the tunneling current is given by [21],

$$I \simeq Ve^{-\frac{2s}{\hbar}\sqrt{2m\Phi}}. \tag{2.5}$$

If small biases are applied between two metals in their normal state the tunneling current I, through insulating film is approximately linear with the applied voltage, as long as the height of the barrier Φ and the density of electron states are essentially constant and the number of electrons which can flow proportionally increases with the voltage. As bias increases further, the effective barrier decreases and thus, the current increases exponentially. At biases greater than $eV = \Phi$ the barrier width at $E = E_F$ starts to decrease with increasing bias and the current increases faster. The effect of temperature is small, for the electron distribution is equal in both side of the insulator, and also kT is much smaller than the barrier height [21].

If one of the metal or both of them are in a superconducting state, the density of electron states varies rapidly with the applied voltage. In such cases, I-V characteristics are nonlinear [22].

The tunneling resistance at low voltages can be written as,

$$R_T \approx exp[(2s/\hbar)(2m\Phi)^{\frac{1}{2}}] \approx exp(-t\Phi^{\frac{1}{2}}) \tag{2.6}$$

where m is the electron mass, $\hbar$ is Planck's constant, s is the separation distance between two electrodes, and Φ is the work function. If the work function is about 4 eV, 1-$\mathring{A}$ change in separation distance, changes the resistance by an order of magnitude [7]. For low voltages the resistivity is constant; at higher voltages the resistivity decreases with the increasing voltage [23].

The curves of tunneling current I, differential resistance $R = \frac{dV}{dI}$, and conductance $G = \frac{dI}{dV}$ are shown in figure 2.8 as a function of voltage.

As temperature increases, some of the electrons thermally excite to the higher energies, it increases the tunneling current (I) and conductance (G) and decreases differential resistance (R) [21].

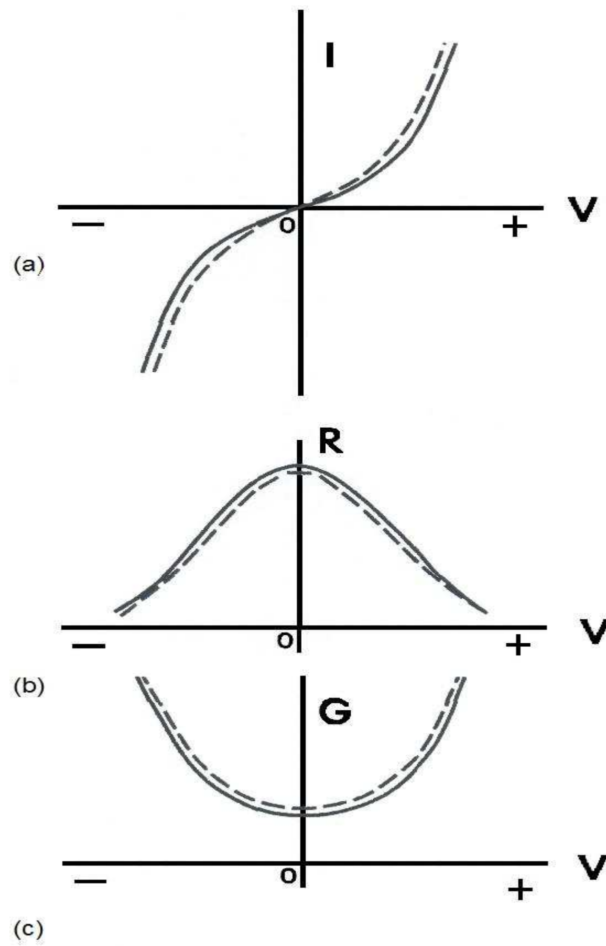

Figure 2.8. Typical curve shapes for free electron (nonsuperconducting state) tunneling at T=0. (a) Current-Voltage (b) Resistance-Voltage (c) Conductance-Voltage. The dashed curves schematically indicate the effect of finite temperature [21].

2.3. Free Electron Tunneling

The basic concepts of tunneling can be understood by studying one of the simplest examples of quantum mechanics: one dimensional square-well.

If the expansion of the tunneling barrier extends in the x direction, the momentum in the y and z direction can usually be taken to be constants of motion [2].

$$E\Psi(x) = \left(-\frac{\hbar^2}{2m}\frac{\partial^2}{\partial x^2} + V \right)\Psi(x). \tag{2.7}$$

The general solution of equation (2.7) is

$$\Psi(x) = ae^{ikx} + be^{-ikx}. \tag{2.8}$$

When $E - V > 0$ the wave functions are plane waves, if $E - V < 0$ we will write $k = i\kappa$ and then,

$$\Psi(x) = ae^{\kappa x} + be^{-\kappa x}. \tag{2.9}$$

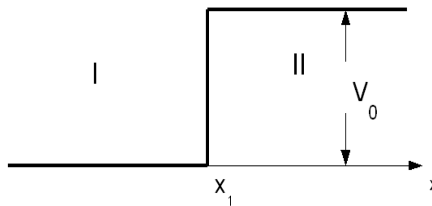

Figure 2.9. A potential step of height V_0

In order to provide the continuity of the probability density, we need to ensure that the wave function and the first derivative of the wave function is continuous everywhere. If dΨ/dx is discontinuous, $d^2\Psi/dx^2$ is infinitive. We have to match Ψ and dΨ/dx at the boundaries. Firstly, we equate the wave functions, and also their derivatives on the two sides of the boundary at $x = x_1$.

The wave functions in region I is $\begin{pmatrix} a_1 \\ b_1 \end{pmatrix}$ and in region II is $\begin{pmatrix} a_2 \\ b_2 \end{pmatrix}$.

$$\begin{pmatrix} a_1 \\ b_1 \end{pmatrix} = R_1 \begin{pmatrix} a_2 \\ b_2 \end{pmatrix} \quad (2.10)$$

$$R_1 = \frac{1}{2k_1} \begin{pmatrix} (k_1 + k_2)exp[i(-k_1 + k_2)x_1] & (k_1 - k_2)exp[i(-k_1 - k_2)x_1] \\ (k_1 - k_2)exp[i(k_1 + k_2)x_1] & (k_1 + k_2)exp[i(k_1 - k_2)x_1] \end{pmatrix} \quad (2.11)$$

The equations (2.10) and (2.11) true for real and imaginary values of k.

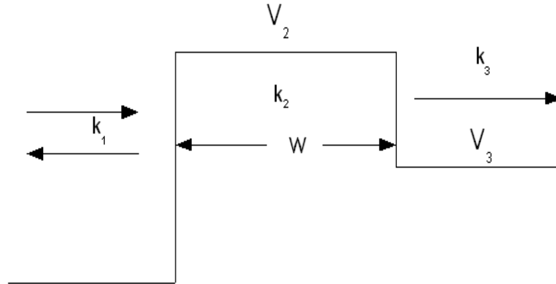

Figure 2.10. Free electron tunneling through one dimensional square-well potential

$$\begin{pmatrix} a_1 \\ b_1 \end{pmatrix} = R_1 R_2 \begin{pmatrix} a_3 \\ b_3 \end{pmatrix} \quad (2.12)$$

where $\begin{pmatrix} a_3 \\ b_3 \end{pmatrix}$ is the wave function in region 3.

There will be only transmitted wave in region 3; therefore b_3 =0.

$$a_1 = (R_1R_2)_{11}a_3 \tag{2.13}$$

If we use equation (2.11) we will have,

$$(R_1R_2)_{11} = [exp(ik_3x_2 - ik_1x_1)](k_1^2 + \kappa_2^2)^{\frac{1}{2}}\frac{(e^{i\alpha}e^{\kappa_2 w} - e^{-i\alpha}e^{-\kappa_2 w})}{4ik_1\kappa_2}. \tag{2.14}$$

$$\alpha = tan^{-1}\left(\frac{\kappa_2}{k_1}\right) + tan^{-1}\left(\frac{\kappa_2}{k_3}\right) \tag{2.15}$$

$$\kappa_2 = ik_2 \qquad \text{and} \qquad w = x_2 - x_1$$

We assume waves in region 1 and 3 are plane waves; to simplify, we neglect e^{-x_2w} in comparison to e^{x_2w}. Then,

$$a_3 = \frac{4k_1\kappa_2\varphi e^{-\kappa_2 w}}{(k_1^2 + \kappa_2^2)^{\frac{1}{2}}(k_3^2 + \kappa_2^2)^{\frac{1}{2}}}a_1. \tag{2.16}$$

$$\varphi = ie^{-i\alpha}exp(ik_1 - ik_3x_2) \tag{2.17}$$

We can compute transmitted current j_3, and incident current j_1

$$j_1 = \left(\frac{\hbar k_1}{m}\right)|a_1|^2; \qquad j_3 = \left(\frac{\hbar k_3}{m}\right)|a_3|^2. \tag{2.18}$$

$$\frac{j_1}{j_3} = \frac{16k_1k_3\kappa_2^2}{(k_1^2 + \kappa_2^2)(k_3^2 + \kappa_2^2)}e^{-2\kappa_2 w} \tag{2.19}$$

The barrier penetration factor $e^{-2\kappa_2 w}$ in equation (2.19) is the dominant feature. In typical problems it may be 10^{-5} - 10^{-10}, so it tends to dominate the pre-factor.

Equation (2.19) also shows that the transmitted current goes continuously to zero, either k_1 or k_3 approaches to zero [24].

The equation above (2.19) is dominated by the exponential factor. The wider is the barrier, the smaller is the tunnel current. We can define κ as,

$$\kappa = \frac{1}{\hbar}[2m(V_2 - E)]^{\frac{1}{2}}. \tag{2.20}$$

The barriers in solids are on the order of one electron volt; by substituting $(V_2 - E)$ into equation (2.20), taking the free electron mass and a current transmission of 10^{-6}, the width of the barrier can be obtained,

$$s = \frac{1}{2\kappa} ln 10^6 \approx 10^{-9} m. \tag{2.21}$$

Looking at the equation (2.21) we can argue that in order to observe tunneling, the width of the barrier should be of the order of 1 nm [3].

Equation (2.19) shows that the barrier transmission is same from right to the left or vice versa. Let's assume that the states on the left and right are quantized in a box and occupied with an occupancy factor f(E). The incident current is

$$\Delta j_1(E) = |a|^2 \frac{\hbar k_1}{m} \frac{dn}{dE} \Delta E f_1(E). \tag{2.22}$$

Box normalization gives $a^2 = 1/L_1$, where L_1 is the length of the box. The density of states in one dimension without spin is

$$\frac{dn}{dE} = \frac{mL_1}{2\pi\hbar^2 k_1}. \tag{2.23}$$

$$\Delta j_1(E) = \frac{f_1(E)}{2\pi\hbar}\Delta E \quad (2.24)$$

The transmitted current per energy is

$$\Delta j_3(E) = \frac{f_3(E)}{2\pi\hbar}\Delta E \quad (2.25)$$

In equilibrium $f_1(E) = f_3(E)$; hence the current per unit energy, incident on both sides of the barrier is same.

2.4. Evaluation of the Tunneling Probability

To evaluate $D(E, k_r)$ we need to solve the Schrödinger equation. We have to match Ψ and $d\Psi/dx$ at the boundaries. Firstly, we equate the wave functions, and also their derivatives on the two sides of the boundary at $x = x_1$. This is difficult in some cases, due to the complexities of the wave function in each region. If we assume that, the metals are made up of free electrons, the problem becomes simpler [21].

A WKB approximation is used for the wave function in the barrier. We consider a normalized wave function Ψ_1^i incident on the left, $R\Psi_1^r$ reflected to the left, and $T\Psi_1^t$ transmitted. Conservation of probability current requires,

$$R^2 + \frac{v_3}{v_1}T^2 = 1 \quad (2.26)$$

where v_1 and v_3 are the electron velocities on both sides of the barrier.

$$D = \frac{v_3}{v_1}T^2 \quad (2.27)$$

If we solve the Schrödinger equation under the above conditions by matching the wave

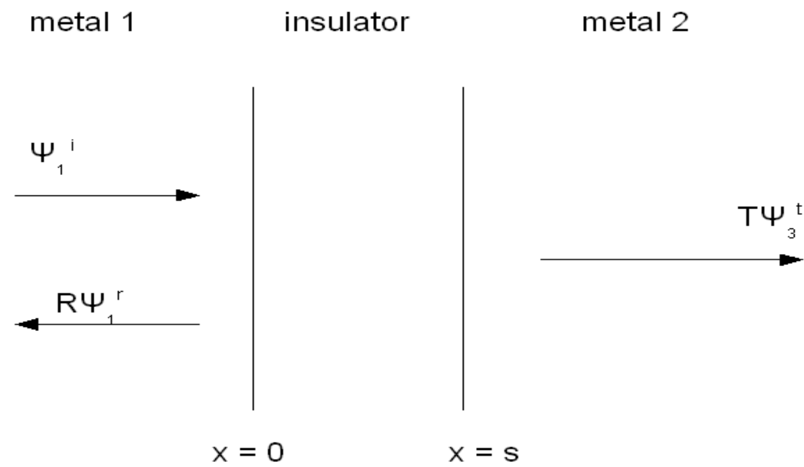

Figure 2.11. General tunneling problem. The wave functions, Ψ and dΨ/dx must be matched at x = 0 and x = s

functions and $\frac{1}{m}\frac{\partial \Psi}{\partial x}$ at $x = 0$ and $x = s$, and evaluating D, we find,

$$D(E_x) = e^{-\frac{4\pi}{\hbar}\int_o^s \sqrt{2m(U(x)-E_x)}dx}. \tag{2.28}$$

2.5. Calculation of the Tunneling Current

The probability $D(E_x)$ that an electron can penetrate a potential barrier of height $V(x)$ -the barrier is assumed to be in the x direction- is given by [25],

$$D(E_x) = e^{-\frac{4\pi}{\hbar}\int_o^s \sqrt{2m(U(x)-E_x)}dx} \tag{2.29}$$

where $E_x = \frac{m{v_x}^2}{2}$, and it is the energy component of the incident electron in the x direction. The number of electrons N_1 tunneling through the barrier from electrode 1

to electrode 2 is given by [26]

$$N_1 = \int_o^{v_m} v_x n(v_x) D(E_x) dv_x = \frac{1}{m} \int_o^{E_m} n(v_x) D(E_x) dE_x \tag{2.30}$$

where E_m is the maximum energy of the electrons in the electrode, and $n(v_x)dv_x$ is the number of electrons per unit volume with velocity between v_x and $v_x + dv_x$. Using the velocity distribution, which is assumed to exist inside the electrodes, the number of electrons per unit volume with velocity between infinitesimal limits is given by

$$n(v) dv_x dv_y dv_z = \frac{2m^4}{h^3} f(E) dv_x dv_y dv_z \tag{2.31}$$

where $f(E)$ is the Fermi-Dirac distribution function. Consequently, from equation (2.31),

$$n(v_x) = \frac{2m^4}{h^3} \int \int_{-\infty}^{\infty} f(E) dv_y dv_z = \frac{4\pi m^3}{h^3} \int_0^{\infty} f(E) dE_r. \tag{2.32}$$

In equation (2.32) integrand is expressed in polar coordinates; that is,

$${v_r}^2 = {v_y}^2 + {v_z}^2.$$

$$E_r = \frac{m{v_r}^2}{2}.$$

Substituting equation (2.32) in (2.31) yields

$$N_1 = \frac{4\pi m^2}{h^3} \int_0^{E_m} D(E_x) dE_x \int_0^{\infty} f(E) dE_r. \tag{2.33}$$

The number of electrons N_2 tunneling from electrode 2 to electrode 1 is determined in a similar manner. The tunneling probability $D(E_x)$ is same in either direction, and if electrode 2 is at a positive potential V with respect to electrode 1, the Fermi-Dirac

function is written as $f(E+eV)$; therefore [26],

$$N_2 = \frac{4\pi m^2}{h^3}\int_0^{E_m} D(E_x)dE_x \int_0^{\infty} f(E+eV)dE_r. \tag{2.34}$$

The net flow of electrons N$(N_1 - N_2)$ through the barrier is

$$N = \int_0^{E_m} D(E_x)dE_x \left\{ \frac{4\pi m^2}{h^3}\int_0^{\infty} [f(E) - f(E+eV)]dE_r \right\} \tag{2.35}$$

writing

$$\zeta_1 = \frac{4\pi m^2 e}{h^3}\int_0^{\infty} f(E)dE_r$$

$$\zeta_2 = \frac{4\pi m^2 e}{h^3}\int_0^{\infty} f(E+eV)dE_r$$

and $\zeta = \zeta_1 - \zeta_2$, equation (2.35) becomes

$$J = \int_0^{E_m} D(E_x)\zeta dE_x. \tag{2.36}$$

2.5.1. The Influence of Image Force

The type of the barrier we study is idealized; in other words, we neglect the image force [27]. When an electron exist between two parallel and closely spaced electrodes it polarizes both of the electrodes. As a result, both of the electrodes influence the potential of the electron within the electrode separation [28]. The effect of the image force is to reduce the area of the potential by rounding off the corners and reducing the thickness of the barrier and hence to increase the flow of current between the electrodes.

Sommerfeld and Bethe's correction to take the image force in account was based on the approximation of the hill by a symmetric parabola. Holm and Kirschstein fit the

parabola closer to the assumed potential hill [6]. This approximation is good only for the low-voltage range and high barriers. When voltage V is applied to the electrodes, the parabola is moved vertically down the energy diagram by an amount $\frac{eV}{2}$. For high voltages, the approximation is poor [26].

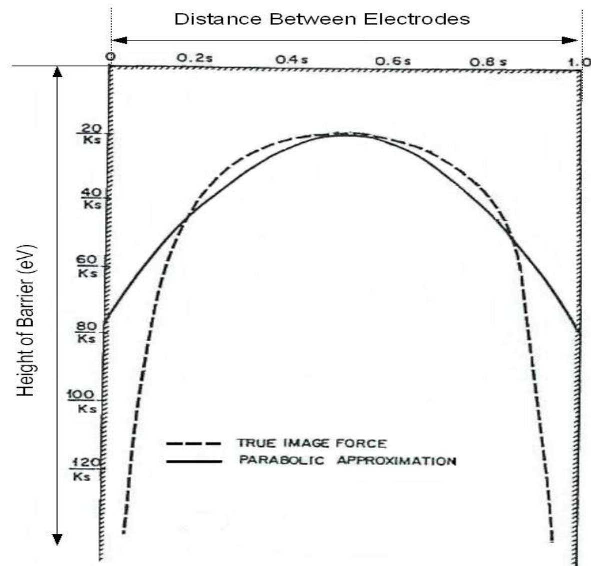

Figure 2.12. Normalized energy diagram comparing a parabolic approximation with true barrier for zero voltage bias [28]

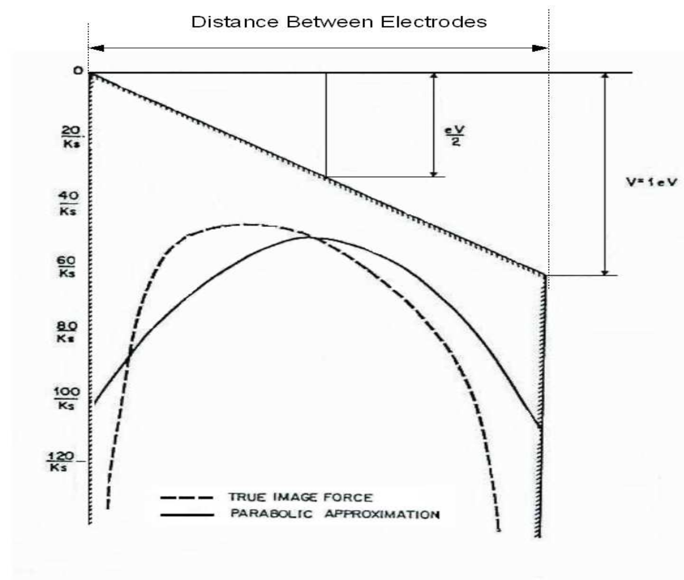

Figure 2.13. Normalized energy diagram comparing a parabolic approximation with true barrier for zero voltage bias of 1 eV [6]

3. EXPERIMENTAL WORK AND RESULTS

3.1. Sample Preparation

The samples consist of glass substrates approximately 25x75 mm. Two metallic electrodes which are separated by a thin oxide layer, have been evaporated on the substrates.

Many types of smooth insulating substrates can be used for M-O-M junctions such as silicone substrates, sapphire substrates, ordinary glass microscope and cover glasses [29]. The microscope slides are found to have smoother surfaces than others, so they are preferred [21].

All the samples are Al-Al_2O_3-Al type. Because of their uniformity and compactness, grown oxides on aluminum or tantalum are generally used [23]. The reason of choosing aluminum is because it is easy to evaporate and is controllable for oxidation. The small atomic size gives us an opportunity of having smaller holes on Al_2O_3. Thus, the characteristics of junction do not change in the length of time. Cr, Ni, Mg, Nb, Ta, Sn, Pb, Ag, Au can be also used as electrodes [2].

The masks with small junction area are preferred to form the electrodes since, small junction area minimizes the chances of having a pinhole in the oxide which may fill with metal from the top electrode and produce shorts [8]. Pollack [30] reported that the evaporation of SiO films over the edges of the Pb film reduces the occurrence of pinhole shorts. These shorts generally occurred at the edges where the evaporated oxide insufficiently insulated the film and where field inhomogeneities were greatest.

The thickness of oxide has to be between $10\AA$ and $30\AA$. If the thickness of oxide is thinner then $10\AA$, there is a high probability to have pinholes in the oxide. If the thickness of oxide is thicker than $30\AA$, then electrons cannot tunnel the barrier.

Due to the uncontrolled impurities in the junction, some of the electrons can tunnel inelastically. In order to prevent inelastic tunneling, there should not be any organic material in the vacuum system and until the evaporation of the second electrode, samples should be kept in the vacuum system [12].

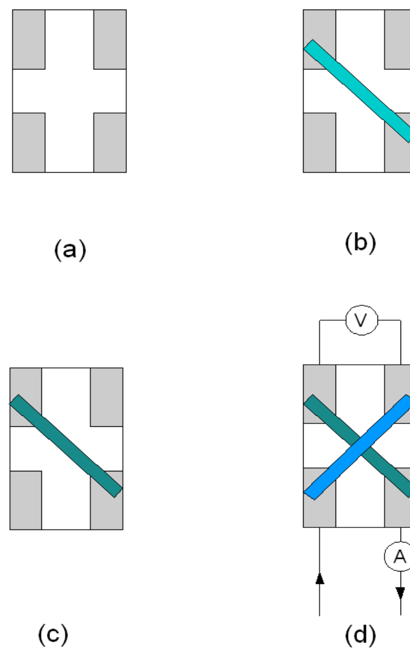

Figure 3.1. Preparation of an Al-Al_2O_3-Al sandwich. (a) Glass slide with indium contacts. (b) An aluminum strip has been deposited across the contacts. (c) The aluminum strip has been oxidized to form an Al_2O_3 layer. (d) A film has been deposited across the film, forming an Al-Al_2O_3-Al sandwich. The external leads are connected to the indium contacts; two contacts are used for the current measurement and two for the voltage measurement [22].

3.1.1. Evaporation

The general preparation procedure of $Al - Al_2O_3 - Al$ junctions is outlined in figure 3.1. The microscope slide is firstly cleaned ultrasonically in alconox detergent. Afterwards, they are rinsed with water, methanol (in order to prevent water absorption) and acetone (in order to remove grease from substrates). We have to minimize water

vapor and grease in the vacuum system to reach lower pressure. All cleaned parts of vacuum system and cleaned substrates should be handled with nylon gloves.

The next step is to apply indium contacts. Indium is used as a solder because it melts relatively low (212 °C) and it sticks nicely to the glass.

The thin films are prepared by using Edwards Coating System, E306A. Thermal evaporation is performed by heating the 99.99% pure aluminum in a tungsten filament.

3.1.2. Oxide Barrier

In metal-oxide-metal junctions the function of oxide is to be a space between electrodes and to prevent any direct contact.

Oxide growth described as the migration of positive metal ions through the oxide. The result of this is a reaction at the boundary between the oxide and oxidizing atmosphere. Another mechanism can be explained as the reaction at the metal oxide interface produced by oxygen ions crossing the oxide film. In both cases electrons diffuse from the metal to the oxidizing atmosphere [5]. Different techniques are used in the oxidation process.

3.1.2.1. Thermal Oxidation. After the evaporation of the first electrode, the slide is removed from the vented system and exposed to atmosphere at various temperatures and humidities. Cleanliness of the air is a key to obtaining good air-oxidized tunnel junctions [29]. Good junctions cannot be obtained on dirty substrates. The different ways of thermal evaporation are:

- to place in a preheated furnace of dry air at atmospheric pressure [31].
- oxidation in room conditions
- to place in distilled water [14]

Oxide films which were grown in atmosphere, were not thick enough to produce tunnel junction of usable resistance. In addition, these films contain a large number of impurities due to the atmospheric pollution. Besides, the thickness of oxide cannot be controlled [29].

Several parameters can play role in this procedure:

- exposure time,
- substrate temperature,
- presence of water vapor and organic impurities

As mentioned below, temperature is an important parameter in an oxidation process. Generally, the rate of a chemical reaction ν increases with the temperature, following the Arrhenius equation.

$$\nu = Cexp(-\frac{E_a}{T}).$$

where C is a constant, E_a is the activation energy [5].

In the M-O-M sandwiches, shorts are frequently observed. During the evaporation of the second electrode, the metals of higher evaporation temperature and hence higher kinetic energy would penetrate into the oxide and reduce the thickness of oxide layer [23].

<u>3.1.2.2. Glow Discharge Oxidation.</u> According to the theory of oxidation, two things are required for the growth of an oxide film on a metal. One is the availability of oxygen and second is the existence of an electric field of proper magnitude and sign at the metal-oxide boundary [32]. The negative charge distribution of the oxygen ions at the oxygen-oxide interface allows the migration of metal ions and produces further growth of the oxide film.

Migration of metal ions can be enhanced with the aid of an externally applied electric field [5].

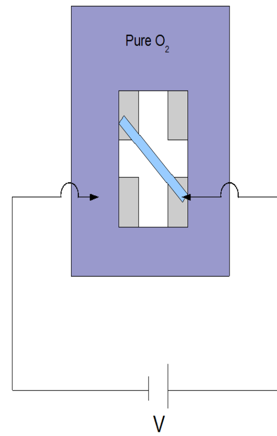

Figure 3.2. The glow discharge oxidation method

The glow discharge method is shown in figure 3.2. The most important advantage of this method is the fabrication of the sample without exposing it to the atmosphere until the end of evaporation. By gas discharge technique, clean oxide layers of controllable thickness were produced [33]. Additionally junction quality, junction resistance and the thickness of oxide are reproducible from sample to sample as well as run to run [8].

Firstly, the indium contacts are applied and the wire is mounted to the vacuum system. As the base electrode is evaporated onto the indium contact, the vacuum system serves as the ground electrode. After the evaporation of the base electrode, oxygen gas is admitted to bring the system to a pressure of about $7x10^{-2}$ mbar, then the high voltage is applied. This produces a glow, which oxidizes the surface of the electrode.

The three oxidation parameters are:

- voltage between the negative electrode and Al film

- time of discharge

- O_2 pressure in the chamber

After the determination of the system parameters, desired junctions can be fabricated again and again. By changing parameters, the thickness can be changed. In order to obtain a relatively thin oxide, the time of discharge should be shortened. However, if the pressure of O_2 is greater than 0.3-0.4 mbar, the mean free path of oxygen molecules decreases [8]. Thus, they do not have enough energy for oxidation when they reach base electrode. Experimentation is necessary since each vacuum system has a different geometry and glow discharge pattern depends on the geometry of the chamber [29].

The oxygen molecules striking the Al surface are more energetic and have more densely packed structure in glow discharge method [8]. The oxide films formed by glow discharge method have been found to be more stable, homogeneous and useful. They are extremely reproducible, and this method allows fine control of thickness.

3.2. Measurement of I-V Characteristics

The samples are mounted to a picoammeter/voltage source (Keithley 487) as shown in figure 3.3. The 487 sources up to 500V (DC), measures the current from 10fA to 2mA. The voltage range between V_{min} and V_{max} scanned by constant increments ΔV at constant time intervals.

3.3. Measurement of Optoelectronic Characteristics

M-O-M systems can be used as electromagnetic detectors. In M-O-M junctions; the thickness, the area and the quality of the junction can be fabricated in desired characteristics and the characteristics of the junctions do not change in time.

In this experiment, my aim was to study the optoelectronic characteristics and to conceive the shape of the junctions. However I could not obtain any logical data from

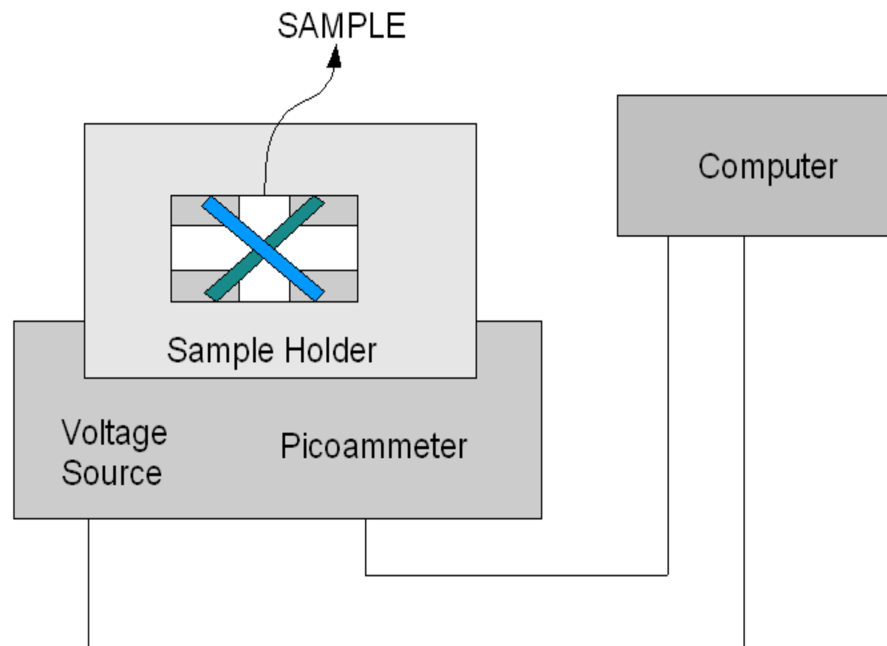

Figure 3.3. The set-up used for I-V measurement

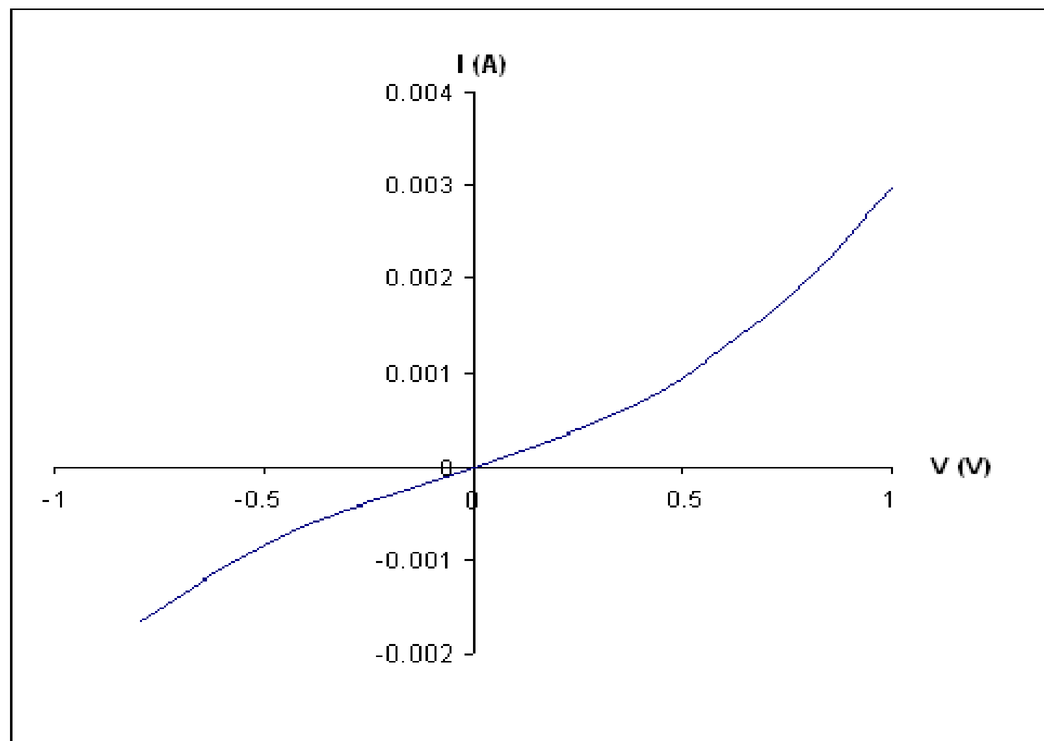

Figure 3.4. I-V characteristics of a typical junction

lock-in amplifier. One of the reason may be the thickness of the insulators. For some of the samples, the thickness of the insulators were too thick for tunneling. For the others, the thickness of the insulators were too thin and thus shorts were frequently observed.

The other reason may be the dept of penetration of the light. The depth of penetration of an electromagnetic wave in a conductor is given by,

$$\delta = \left(\frac{2}{w\sigma\mu}\right)^{\frac{1}{2}}$$

where μ ($\mu_{Al} = 1.26x10^{-6}\ N/A^2$) is the permeability constant, σ ($\sigma_{Al} = 3.54x10^7$ mho/m) is the conductivity and w is the frequency of the wave. If we calculate depth of penetration of the wave (w=$4.5x10^{14}$ Hz) in aluminum we would find that the wave can penetrate $100\AA$. If the thickness of the upper electrode is thicker than $100\AA$, the wave cannot reach the base electrode. Al_2O_3 transmits light perfectly. The assumed shape of the junction is given in figure 3.8. To prove this argument, we would cover the edges of the upper electrode with Al films -the thickness should be $2000\AA$- (See Figure 3.9). To prevent shorts, an insulator like formvar could be used. Formvar is transparent and a good insulator in high fields. If the assumption is true, the tunneling current cannot be detected. We could conclude that the effective area of the junctions is the edges of the upper electrode[12].

3.3.1. Lock-in Amplifiers

Lock-in amplifiers are used to detect and measure very small AC signals, buried in noise. They achieve this by acting as a narrow bandpass filter which removes much of the unwanted noise while allowing through the signal which is to be measured. Lock-in amplifier rejects the noise signal at frequencies other than the reference frequency by using phase sensitive detection.

In this set-up, we used a continuous laser to induce the signal of interest which is modulated by a chopper. The amplifier measures the amplitude and phase of the

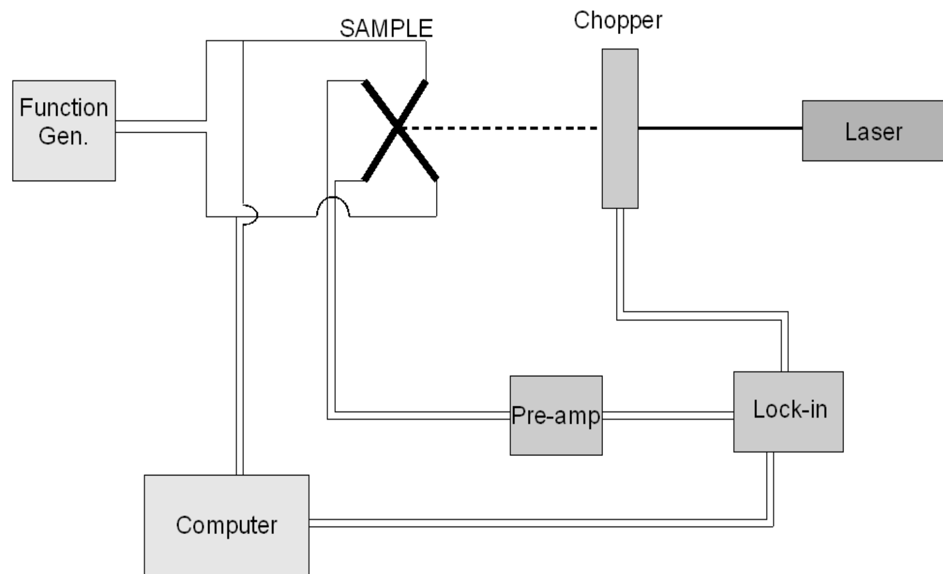

Figure 3.5. The set-up used for the measurement of the optoelectronic characteristics

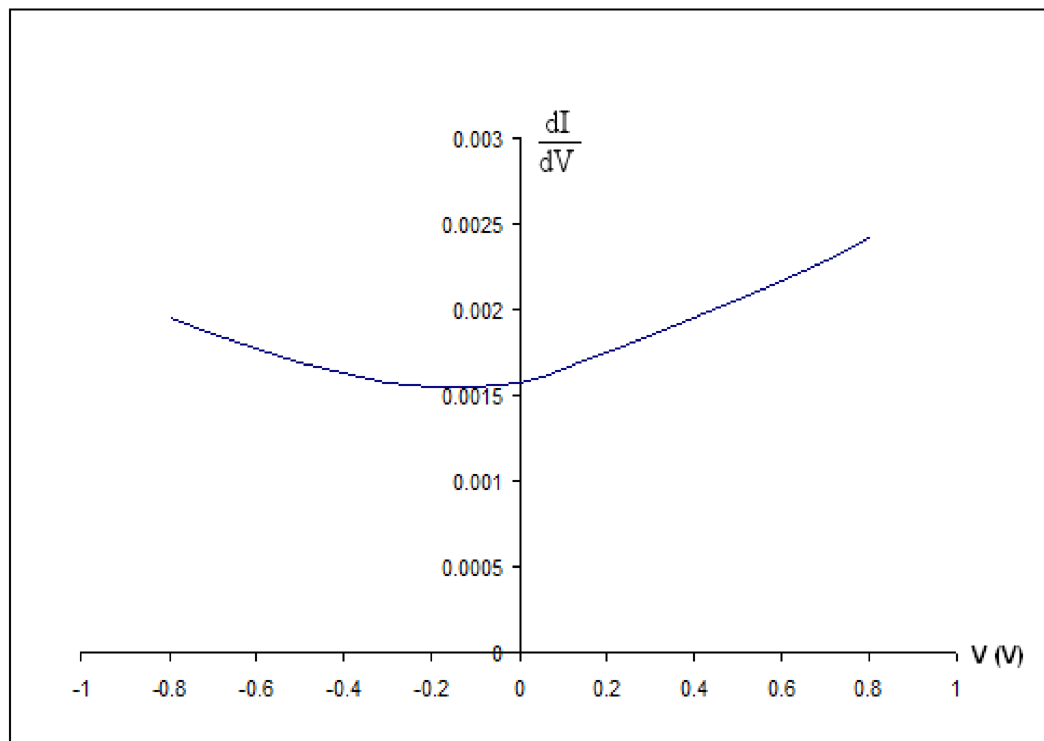

Figure 3.6. dI/dV vs V for a typical junction

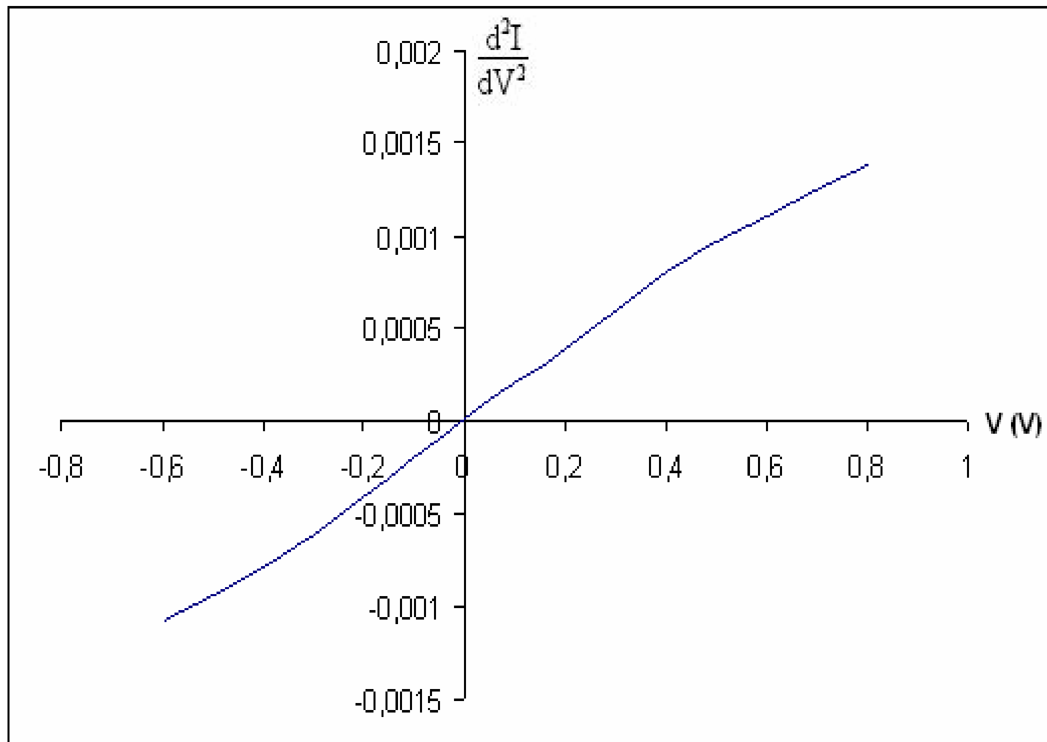

Figure 3.7. $d^2I/dV^2 vs V$ for a typical junction

signal of interest relative to a reference output from the chopper. The power of the laser is proportional to the AC potential on the junction.

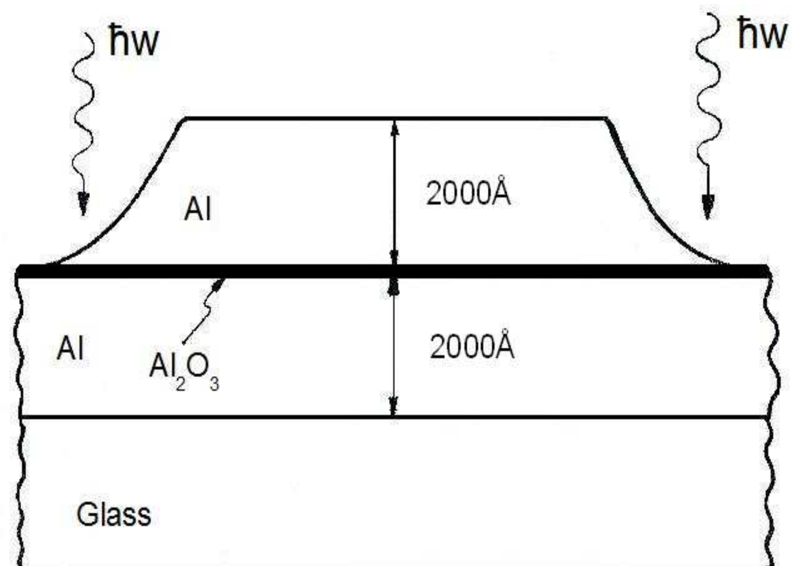

Figure 3.8. The assumed shape of the junction[12]

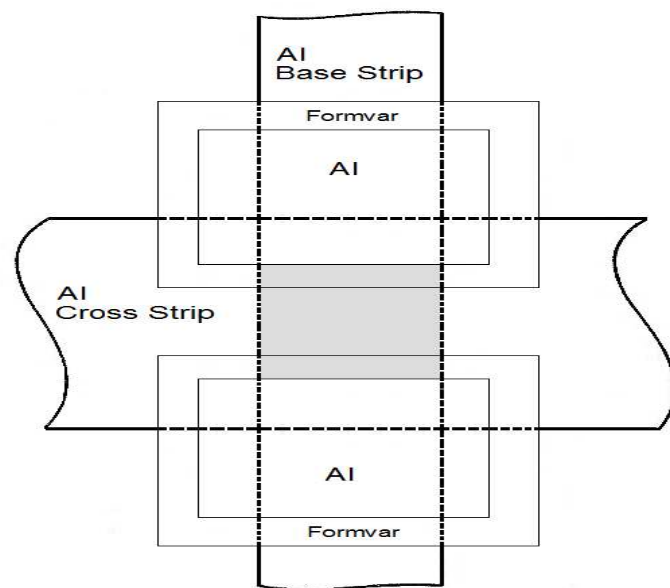

Figure 3.9. The edges of the junction is covered with Al films[12]

4. CONCLUSION

In this thesis, an attempt has been made to detect the optical frequencies of $Al - Al_2O_3 - Al$ junctions. It seems certain that the observed conductivity in the aluminum oxide films is because of the tunneling of electrons through the films.

The thin films obtained through a number of different oxidation techniques: some were oxidized in air, some in oxygen atmosphere at various temperatures, some in distilled water and some were oxidized by glow discharge method to form an oxide layer.

In thermal oxidation; the oxide films were grown on the Al strip by exposing it to air at some temperature T, during a time t. T is varied from 23 °C to 250 °C and t is ranged from 1 h to 1000 h. Some of the slides were placed in distilled water for 10 h. However shorts were frequently observed in the junctions that were prepared through these methods, except the glow discharge method.

The current-voltage relationship and the basic characteristics of the tunneling current are described in theory. The current-voltage characteristics of $Al - Al_2O_3 - Al$ sample is shown in figure 3.4, and this is in agreement with the theoretically expected characteristics for tunneling current.

The results of the measurements in $Al - Al_2O_3 - Al$ films (which were prepared through evaporating an Al strip onto a glass substrate, then allowing the film to oxidize and finally evaporating a cross strip of Al over the oxide at a vacuum in the range of 10^{-5} mbar) are in accordance with the theoretical and experimental works of previous investigators.

REFERENCES

1. O'reilly, E.P., *Quantum Theory in Solids*, CRC Press, London, 2002.

2. Duke, C.B., *Tunneling in Solids*, Academic Press, New York, 1969.

3. Solymar, L., *Superconductive Tunneling and Applications*, Chapman and Hall LTD, London, 1972.

4. Razavy, M., *Quantum Theory of Tunneling*, World Scientific, River Edge NJ, 2003.

5. Barone, A., Paternò, G., *Physics and Applications of the Josephson Effect*, John Wiley, New York, 1982.

6. Simmons, J.G, "Electric tunel effect between dissimilar electrodes separated by a thin insulating film", *Journal of Applied Physics*, Vol. 34, pp. 2581-2590, 1963.

7. Giaever, I., *Tunneling Phenomena in Solids (E.Burnstein and S. Lundquist, Eds.)*, Plenum Press, New York, 1969.

8. Skarlatos, Y., "*Inelastic Electron Tunneling Spectroscopy as a Tool in Water Analysis*", Phd Thesis, Yale University, 1974.

9. Jaklevic, R.C., Lambe J., *Tunneling Phenomena in Solids (E.Burnstein and S. Lundquist, Eds.)*, Plenum Press, New York, 1969.

10. Klein, J., Léger A., Belin M., Défourneau D., Sangster, M.J.L., "Inelastic-electron-tunneling spectroscopy of metal-insulator-metal juctions", *Physical Review B*, Vol. 7, pp. 2336-2348, 1973.

11. Lambe, J. Jaklevic, R.C., *Tunneling Phenomena in Solids (E.Burnstein and S. Lundquist, Eds.)*, Plenum Press, New York, 1969.

12. Skarlatos, Y., *Görülen Işığa Duyarlı, İnce Filmle Yapılmış Bir Optoelektronik Aygıt*, Assoc.Prof. Thesis, Bogazici University, 1978.

13. Lambe, J., Jaklevic, R.C., "Molecular vibrations spectra by inelastic electron tunneling", *Physical Review*, Vol. 165, pp. 821-832, 1968.

14. Fischer, J.C., Giaever, I., "Tunneling through thin insulating layers", *Journal of Applied Physics*, Vol. 32, pp. 172-177, 1961.

15. Meyerhofer, D., Ochs, S.A., "Current flow in very thin films of Al_2O_3 and BeO", *Journal of Applied Physics*, Vol. 34, pp. 2535-2543, 1963.

16. Stratton, R., *Tunneling Phenomena in Solids (E.Burnstein and S. Lundquist, Eds.)*, Plenum Press, New York, 1969.

17. Christov, S.G., "Electron currents through barriers between two metals", *Contemporary Physics*, Vol. 13, pp. 199-222, 1972.

18. Simmons, J.G, "Generalized thermal J-V characteristic for the electric tunel effect ", *Journal of Applied Physics*, Vol. 35, pp. 2655-2658, 1964.

19. Simmons, J.G, "Intrinsic fields in thin insulating films between dissimilar electrodes", *Physical Review Letters*, Vol. 10, pp. 10-12, 1963.

20. Simmons, J.G, "Potential barriers and emission-limited current flow between closely spaced parallel metal electrodes", *Journal of Applied Physics*, Vol. 35, pp. 2472-2481, 1964.

21. Grant, Westley N., *"Electron Tunneling in Aluminum-Insulator-Palladium, Silver Junctions"*, Phd. Thesis, Yale University, 1970.

22. Giaever, I., Megerle, K., "Study of superconductors by electron tunneling", *Physical Review*, Vol. 122, pp. 1101-1111, 1961.

23. Handy, R.M, "Electrode efects on auminum oxide tunnel junctions", *Physical Review*, Vol. 126, pp. 1968-1973, 1962.

24. Kane, E.O., *Tunneling Phenomena in Solids (E.Burnstein and S. Lundquist, Eds.)*, Plenum Press, New York, 1969.

25. Holm, R., "The electric tunnel effect across thin insulator films in contact", *Journal of Applied Physics*, Vol. 22, pp. 569-573, 1951.

26. Simmons, J.G, "Generalized formula for the electric tunnel effect between similar electrodes separated by a thin insulating film", *Journal of Applied Physics*, Vol. 34, pp. 1793-1802,1963.

27. Simmons, J.G., Unterkofler, G.J., "Potential barrier shape determination in tunnel junction", *Journal of Applied Physics*, Vol. 34, pp. 1828-1830, 1962.

28. Simmons, J.G., *Tunneling Phenomena in Solids (E.Burnstein and S. Lundquist, Eds.)*, Plenum Press, New York, 1969.

29. Hansma, P.K., *Tunneling Spectroscopy*, Plenum Press, New York, 1982.

30. Pollack, S.R., "Schottky field emission through insulating layers", *Journal of Applied Physics*, Vol. 34, pp. 877-880, 1963.

31. Hartman, T.E., "Electron tunneling through thin aluminum oxide films", *Physical Review*, Vol. 134, pp. A1094-A1101, 1964.

32. Miles, J.L., Smith, P.H.,"The formation of metal oxide films using gaseous and solid electrolytes", *Journal of The Electrochemical Society*, Vol. 110, pp. 1240-1245, 1963.

33. Geiger, A.L, Chandrasekhar, B.S., "Inelastic electron tunneling in Al-Al-Oxide-Metal systems", *Physical Review*, Vol. 188, pp. 1130-1138, 1969.